Event-by-event fluctuations in mean p_T and mean e_T in $\sqrt{s_{NN}}$=130 GeV Au+Au collisions

K. Adcox,[40] S. S. Adler,[3] N. N. Ajitanand,[27] Y. Akiba,[14] J. Alexander,[27] L. Aphecetche,[34] Y. Arai,[14] S. H. Aronson,[3] R. Averbeck,[28] T. C. Awes,[29] K. N. Barish,[5] P. D. Barnes,[19] J. Barrette,[21] B. Bassalleck,[25] S. Bathe,[22] V. Baublis,[30] A. Bazilevsky,[12,32] S. Belikov,[12,13] F. G. Bellaiche,[29] S. T. Belyaev,[16] M. J. Bennett,[19] Y. Berdnikov,[35] S. Botelho,[33] M. L. Brooks,[19] D. S. Brown,[26] N. Bruner,[25] D. Bucher,[22] H. Buesching,[22] V. Bumazhnov,[12] G. Bunce,[3,32] J. Burward-Hoy,[28] S. Butsyk,[28,30] T. A. Carey,[19] P. Chand,[2] J. Chang,[5] W. C. Chang,[1] L. L. Chavez,[25] S. Chernichenko,[12] C. Y. Chi,[8] J. Chiba,[14] M. Chiu,[8] R. K. Choudhury,[2] T. Christ,[28] T. Chujo,[3,39] M. S. Chung,[15,19] P. Chung,[27] V. Cianciolo,[29] B. A. Cole,[8] D. G. D'Enterria,[34] G. David,[3] H. Delagrange,[34] A. Denisov,[12] A. Deshpande,[32] E. J. Desmond,[3] O. Dietzsch,[33] B. V. Dinesh,[2] A. Drees,[28] A. Durum,[12] D. Dutta,[2] K. Ebisu,[24] Y. V. Efremenko,[29] K. El Chenawi,[40] H. En'yo,[17,31] S. Esumi,[39] L. Ewell,[3] T. Ferdousi,[5] D. E. Fields,[25] S. L. Fokin,[16] Z. Fraenkel,[42] A. Franz,[3] A. D. Frawley,[9] S.-Y. Fung,[5] S. Garpman,[20,*] T. K. Ghosh,[40] A. Glenn,[36] A. L. Godoi,[33] Y. Goto,[32] S. V. Greene,[40] M. Grosse Perdekamp,[32] S. K. Gupta,[2] W. Guryn,[3] H.-Å. Gustafsson,[20] J. S. Haggerty,[3] H. Hamagaki,[7] A. G. Hansen,[19] H. Hara,[24] E. P. Hartouni,[18] R. Hayano,[38] N. Hayashi,[31] X. He,[10] T. K. Hemmick,[28] J. M. Heuser,[28] M. Hibino,[41] J. C. Hill,[13] D. S. Ho,[43] K. Homma,[11] B. Hong,[15] A. Hoover,[26] T. Ichihara,[31,32] K. Imai,[17,31] M. S. Ippolitov,[16] M. Ishihara,[31,32] B. V. Jacak,[28,32] W. Y. Jang,[15] J. Jia,[28] B. M. Johnson,[3] S. C. Johnson,[18,28] K. S. Joo,[23] S. Kametani,[41] J. H. Kang,[43] M. Kann,[30] S. S. Kapoor,[2] S. Kelly,[8] B. Khachaturov,[42] A. Khanzadeev,[30] J. Kikuchi,[41] D. J. Kim,[43] H. J. Kim,[43] S. Y. Kim,[43] Y. G. Kim,[43] W. W. Kinnison,[19] E. Kistenev,[3] A. Kiyomichi,[39] C. Klein-Boesing,[22] S. Klinksiek,[25] L. Kochenda,[30] V. Kochetkov,[12] D. Koehler,[25] T. Kohama,[11] D. Kotchetkov,[5] A. Kozlov,[42] P. J. Kroon,[3] K. Kurita,[31,32] M. J. Kweon,[15] Y. Kwon,[43] G. S. Kyle,[26] R. Lacey,[27] J. G. Lajoie,[13] J. Lauret,[27] A. Lebedev,[13,16] D. M. Lee,[19] M. J. Leitch,[19] X. H. Li,[5] Z. Li,[6,31] D. J. Lim,[43] M. X. Liu,[19] X. Liu,[6] Z. Liu,[6] C. F. Maguire,[40] J. Mahon,[3] Y. I. Makdisi,[3] V. I. Manko,[16] Y. Mao,[6,31] S. K. Mark,[21] S. Markacs,[8] G. Martinez,[34] M. D. Marx,[28] A. Masaike,[17] F. Matathias,[28] T. Matsumoto,[7,41] P. L. McGaughey,[19] E. Melnikov,[12] M. Merschmeyer,[22] F. Messer,[28] M. Messer,[3] Y. Miake,[39] T. E. Miller,[40] A. Milov,[42] S. Mioduszewski,[3,36] R. E. Mischke,[19] G. C. Mishra,[10] J. T. Mitchell,[3] A. K. Mohanty,[2] D. P. Morrison,[3] J. M. Moss,[19] F. Mühlbacher,[28] M. Muniruzzaman,[5] J. Murata,[31] S. Nagamiya,[14] Y. Nagasaka,[24] J. L. Nagle,[8] Y. Nakada,[17] B. K. Nandi,[5] J. Newby,[36] L. Nikkinen,[21] P. Nilsson,[20] S. Nishimura,[7] A. S. Nyanin,[16] J. Nystrand,[20] E. O'Brien,[3] C. A. Ogilvie,[13] H. Ohnishi,[3,11] I. D. Ojha,[4,40] M. Ono,[39] V. Onuchin,[12] A. Oskarsson,[20] L. Österman,[20] I. Otterlund,[20] K. Oyama,[7,38] L. Paffrath,[3,*] A. P. T. Palounek,[19] V. S. Pantuev,[28] V. Papavassiliou,[26] S. F. Pate,[26] T. Peitzmann,[22] A. N. Petridis,[13] C. Pinkenburg,[3,27] R. P. Pisani,[3] P. Pitukhin,[12] F. Plasil,[29] M. Pollack,[28,36] K. Pope,[36] M. L. Purschke,[3] I. Ravinovich,[42] K. F. Read,[29,36] K. Reygers,[22] V. Riabov,[30,35] Y. Riabov,[30] M. Rosati,[13] A. A. Rose,[40] S. S. Ryu,[43] N. Saito,[31,32] A. Sakaguchi,[11] T. Sakaguchi,[7,41] H. Sako,[39] T. Sakuma,[31,37] V. Samsonov,[30] T. C. Sangster,[18] R. Santo,[22] H. D. Sato,[17,31] S. Sato,[39] S. Sawada,[14] B. R. Schlei,[19] Y. Schutz,[34] V. Semenov,[12] R. Seto,[5] T. K. Shea,[3] I. Shein,[12] T.-A. Shibata,[31,37] K. Shigaki,[14] T. Shiina,[19] Y. H. Shin,[43] I. G. Sibiriak,[16] D. Silvermyr,[20] K. S. Sim,[15] J. Simon-Gillo,[19] C. P. Singh,[4] V. Singh,[4] M. Sivertz,[3] A. Soldatov,[12] R. A. Soltz,[18] S. Sorensen,[29,36] P. W. Stankus,[29] N. Starinsky,[21] P. Steinberg,[8] E. Stenlund,[20] A. Ster,[44,†] S. P. Stoll,[3] M. Sugioka,[31,37] T. Sugitate,[11] J. P. Sullivan,[19] Y. Sumi,[11] Z. Sun,[6] M. Suzuki,[39] E. M. Takagui,[33] A. Taketani,[31] M. Tamai,[41] K. H. Tanaka,[14] Y. Tanaka,[24] E. Taniguchi,[31,37] M. J. Tannenbaum,[3] J. Thomas,[28] J. H. Thomas,[18] T. L. Thomas,[25] W. Tian,[6,36] J. Tojo,[17,31] H. Torii,[17,31] R. S. Towell,[19] I. Tserruya,[42] H. Tsuruoka,[39] A. A. Tsvetkov,[16] S. K. Tuli,[4] H. Tydesjö,[20] N. Tyurin,[12] T. Ushiroda,[24] H. W. van Hecke,[19] C. Velissaris,[26] J. Velkovska,[28] M. Velkovsky,[28] A. A. Vinogradov,[16] M. A. Volkov,[16] A. Vorobyov,[30] E. Vznuzdaev,[30] H. Wang,[5] Y. Watanabe,[31,32] S. N. White,[3] C. Witzig,[3] F. K. Wohn,[13] C. L. Woody,[3] W. Xie,[5,42] K. Yagi,[39] S. Yokkaichi,[31] G. R. Young,[29] I. E. Yushmanov,[16] W. A. Zajc,[8] Z. Zhang,[28] and S. Zhou[6]

(PHENIX Collaboration)

[1]*Institute of Physics, Academia Sinica, Taipei 11529, Taiwan*
[2]*Bhabha Atomic Research Centre, Bombay 400 085, India*
[3]*Brookhaven National Laboratory, Upton, New York, 11973-5000*
[4]*Department of Physics, Banaras Hindu University, Varanasi 221005, India*
[5]*University of California–Riverside, Riverside, California 92521*
[6]*China Institute of Atomic Energy (CIAE), Beijing, People's Republic of China*
[7]*Center for Nuclear Study, Graduate School of Science, University of Tokyo, 7-3-1 Hongo, Bunkyo, Tokyo 113-0033, Japan*
[8]*Columbia University, New York, New York 10027*
and Nevis Laboratories, Irvington, New York 10533
[9]*Florida State University, Tallahassee, Florida 32306*
[10]*Georgia State University, Atlanta, Georgia 30303*
[11]*Hiroshima University, Kagamiyama, Higashi-Hiroshima 739-8526, Japan*
[12]*Institute for High Energy Physics (IHEP), Protvino, Russia*
[13]*Iowa State University, Ames, Iowa 50011*
[14]*KEK, High Energy Accelerator Research Organization, Tsukuba-shi, Ibaraki-ken 305-0801, Japan*

[15]*Korea University, Seoul, 136-701, Korea*
[16]*Russian Research Center "Kurchatov Institute," Moscow, Russia*
[17]*Kyoto University, Kyoto 606, Japan*
[18]*Lawrence Livermore National Laboratory, Livermore, California 94550*
[19]*Los Alamos National Laboratory, Los Alamos, New Mexico 87545*
[20]*Department of Physics, Lund University, Box 118, SE-221 00 Lund, Sweden*
[21]*McGill University, Montreal, Quebec, Canada H3A 2T8*
[22]*Institut für Kernphysik, University of Münster, D-48149 Münster, Germany*
[23]*Myongji University, Yongin, Kyonggido 449-728, Korea*
[24]*Nagasaki Institute of Applied Science, Nagasaki-shi, Nagasaki 851-0193, Japan*
[25]*University of New Mexico, Albuquerque, New Mexico 87131*
[26]*New Mexico State University, Las Cruces, New Mexico 88003*
[27]*Chemistry Department, State University of New York–Stony Brook, Stony Brook, New York 11794*
[28]*Department of Physics and Astronomy, State University of New York–Stony Brook, Stony Brook, New York 11794*
[29]*Oak Ridge National Laboratory, Oak Ridge, Tennessee 37831*
[30]*PNPI, Petersburg Nuclear Physics Institute, Gatchina, Russia*
[31]*RIKEN (The Institute of Physical and Chemical Research), Wako, Saitama 351-0198, Japan*
[32]*RIKEN BNL Research Center, Brookhaven National Laboratory, Upton, New York 11973-5000*
[33]*Universidade de São Paulo, Instituto de Física, Caixa Postal 66318, São Paulo CEP05315-970, Brazil*
[34]*SUBATECH (Ecole des Mines de Nantes, IN2P3/CNRS, Universite de Nantes) Boîte Postale 20722-44307, Nantes-cedex 3, France*
[35]*St. Petersburg State Technical University, St. Petersburg, Russia*
[36]*University of Tennessee, Knoxville, Tennessee 37996*
[37]*Department of Physics, Tokyo Institute of Technology, Tokyo, 152-8551, Japan*
[38]*University of Tokyo, Tokyo, Japan*
[39]*Institute of Physics, University of Tsukuba, Tsukuba, Ibaraki 305, Japan*
[40]*Vanderbilt University, Nashville, Tennesse 37235*
[41]*Waseda University, Advanced Research Institute for Science and Engineering, 17 Kikui-cho, Shinjuku-ku, Tokyo 162-0044, Japan*
[42]*Weizmann Institute, Rehovot 76100, Israel*
[43]*Yonsei University, IPAP, Seoul 120-749, Korea*
[44]*KFKI Research Institute for Particle and Nuclear Physics (RMKI), Budapest, Hungary*
(Received 22 March 2002; published 2 August 2002)

Distributions of event-by-event fluctuations of the mean transverse momentum and mean transverse energy near mid-rapidity have been measured in Au+Au collisions at $\sqrt{s_{NN}}=130$ GeV at the Relativistic Heavy-Ion Collider. By comparing the distributions to what is expected for statistically independent particle emission, the magnitude of nonstatistical fluctuations in mean transverse momentum is determined to be consistent with zero. Also, no significant nonrandom fluctuations in mean transverse energy are observed. By constructing a fluctuation model with two event classes that preserve the mean and variance of the semi-inclusive p_T or e_T spectra, we exclude a region of fluctuations in $\sqrt{s_{NN}}=130$ GeV Au+Au collisions.

DOI: 10.1103/PhysRevC.66.0149XX PACS number(s): 25.75.Dw

I. INTRODUCTION

Phase instabilities near the QCD phase transition can result in nonstatistical fluctuations that are detectable in final state observables [1]. These instabilities, which may occur due to random color fluctuations [2], critical behavior at the QCD tricritical point [3], or fluctuations from the decay of a Polyakov loop condensate [4], can result in a broadening of the transverse momentum or transverse energy distributions of particles produced for different classes of events. This phenomenon is expected to be detected experimentally by searching for deviations of the distributions of the event-by-event mean transverse momentum M_{p_T} or mean transverse energy M_{e_T} of produced particles from the random distributions expected for statistically independent particle emission.

An event-by-event analysis of M_{p_T} was previously performed for 158 A GeV/c Pb+Pb collisions at the CERN SPS by Experiment NA49 [5]. In that analysis, the M_{p_T} distributions measured over the rapidity range $4<y_\pi<5.5$ and p_T range $0.005<p_T<1.5$ GeV/c were found to be consistent with random fluctuations. NA49 also performed an event-by-event analysis of the K/π ratio [6], showing only very small deviations from random fluctuations. With an increase of $\sqrt{s_{NN}}$ to 130 GeV in Relativistic Heavy-Ion Collider (RHIC) collisions, unprecedented energy densities have been observed [10]; hence conditions may be more favorable for a phase transition from hadronic matter to a quark-gluon

*Deceased.
†Author is an individual participant.

TABLE I. Statistics pertaining to the M_{p_T} analysis. The values of $\langle M_{p_T} \rangle$ are quoted for $0.2 < p_T < 1.5$ GeV/c and are not corrected for efficiency or acceptance.

Centrality	0–5 %	0–10 %	10–20 %	20–30 %
		Data		
N_{events}	72 692	149 236	149 725	150 365
$\langle N_{tracks} \rangle$	59.6	53.9	36.6	25.0
$\sigma_{N_{tracks}}$	10.8	12.2	10.2	7.8
$\langle M_{p_T} \rangle$ (MeV/c)	523	523	523	520
σ_{p_T} (MeV/c)	290	290	290	289
$\sigma_{M_{p_T}}$ (MeV/c)	38.6	41.1	49.8	61.1
		Mixed events		
$\langle M_{p_T} \rangle$ (MeV/c)	523	523	523	520
$\sigma_{M_{p_T}}$ (MeV/c)	37.8	40.3	48.8	60.0

plasma which may be indicated in nonrandom fluctuations. Presented here is an event-by-event analysis of M_{p_T} fluctuations and the first measurement of M_{e_T} fluctuations at midrapidity at the RHIC.

II. ANALYSIS

The PHENIX Experiment [7] consists of four spectrometers designed to measure simultaneously hadrons, leptons, and photons produced in nucleus-nucleus, proton-nucleus, and proton-proton collisions at RHIC. The two central arm spectrometers, which are located within a focusing magnetic field, each covering ± 0.35 in pseudorapidity and $\Delta\phi = 90°$ in azimuthal angle, are utilized in this analysis. The primary interaction trigger was defined using the Beam-Beam Counters (BBCs) [8] and Zero Degree Calorimeters (ZDCs) [9]. Events are selected with a requirement that the collision vertex along the beam axis has $|z| < 20$ cm as measured by both the BBCs and ZDCs. Event centrality is defined using correlations in the BBC and ZDC analog response as described in [10]. For the present analysis, the events are classified according to the 0–5 %, 0–10 %, 10–20 %, and 20–30 % most central events.

The drift chamber [11] is used in conjunction with the innermost pad chamber, called PC1, to measure the transverse momentum of charged particles traversing the PHENIX acceptance. A fiducial section of the drift chamber is chosen to minimize the effect of time-dependent variations in the performance of the detector during the data-taking period. The fiducial volume of the M_{p_T} analysis spans an azimuthal range of $\Delta\phi = 58.5°$ and covers the pseudorapidity range $|\eta| < 0.35$. Reconstructed tracks [12] are required to contain a match to a hit in PC1 to ensure that the tracks are well reconstructed in three dimensions for reliable momentum determination.

The M_{e_T} distribution is determined from clusters reconstructed in the two instrumented sectors of the lead-scintillator electromagnetic calorimeter [7,13,14]. The quantity e_T is defined as the transverse energy per reconstructed calorimeter cluster as described in [14], which can include clusters that have been merged. The effects of cluster merging on the M_{e_T} distribution are discussed later. The fiducial volume of the M_{e_T} analysis spans an azimuthal range of $\Delta\phi = 45°$ and covers $|\eta| < 0.35$.

There are no acceptance or efficiency corrections applied to the semi-inclusive p_T or e_T distributions prior to the calculation of M_{p_T} or M_{e_T}. Here, the term semi-inclusive refers to spectra in p_T or e_T summed over all events in a given centrality class. These corrections do not vary from event to

TABLE II. Statistics pertaining to the M_{e_T} analysis. The values of $\langle M_{e_T} \rangle$ are quoted for $0.225 < e_T < 2.0$ GeV and are not corrected for efficiency or acceptance.

Centrality	0–5 %	0–10 %	10–20 %	20–30 %
		Data		
N_{events}	69 224	138 882	140 461	137 867
$\langle N_{clus} \rangle$	68.6	62.1	41.6	28.0
$\sigma_{N_{clus}}$	11.6	13.2	10.8	8.3
$\langle M_{e_T} \rangle$ (MeV)	466	462	448	439
σ_{e_T} (MeV)	267	265	258	253
$\sigma_{M_{e_T}}$ (MeV)	34.1	36.2	43.0	51.8
		Mixed Events		
$\langle M_{e_T} \rangle$ (MeV)	466	462	448	439
$\sigma_{M_{e_T}}$ (MeV)	32.7	34.4	41.3	50.0

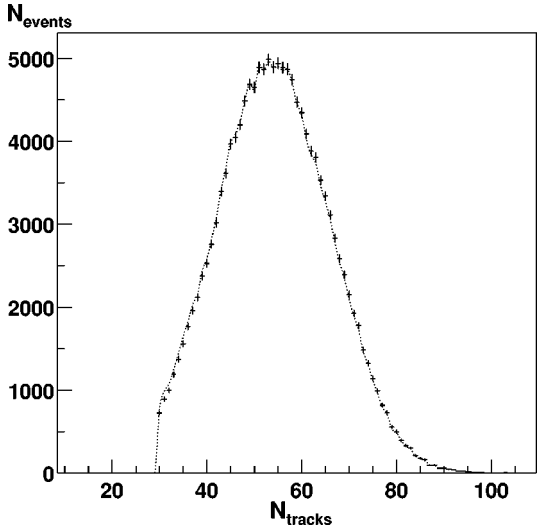

FIG. 1. The N_{tracks} distribution for the 0–10 % centrality class (data points) compared to the N_{mix} distribution from the mixed event sample (curve). Very good agreement in the data and mixed event N_{tracks} distribution is required for a precise comparison of the corresponding M_{p_T} distributions shown in Fig. 3 below.

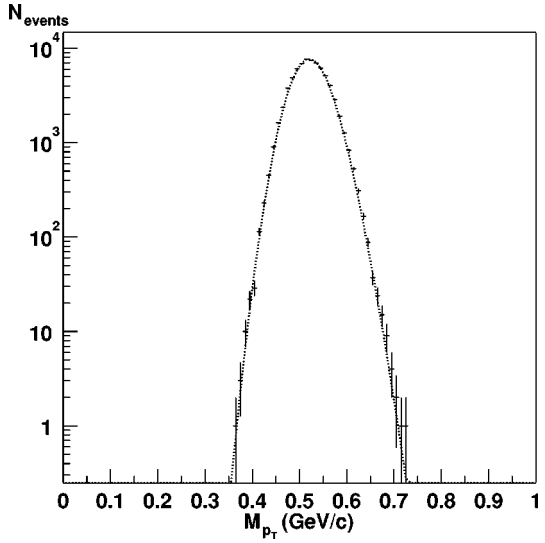

FIG. 2. The M_{p_T} distribution for the 0–5 % centrality class. The curve is the result of a Γ distribution calculation with parameters taken from the semi-inclusive p_T spectra.

event and are identical for data and mixed events (defined below); therefore they do not modify the values of the fluctuation quantities defined later. The M_{p_T} distributions are calculated using the formula

$$M_{p_T}=(1/N_{tracks})\sum_{i=1}^{N_{tracks}} p_{Ti}, \tag{2.1}$$

where N_{tracks} is the number of tracks in the event that pass the cuts outlined above and lie within the p_T range $0.2<p_T<1.5$ GeV/c. Similarly, the M_{e_T} distributions are calculated using the formula

$$M_{e_T}=(1/N_{clus})\sum_{i=1}^{N_{clus}} e_{Ti}, \tag{2.2}$$

where N_{clus} is the number of calorimeter clusters in the event that lie within the e_T range $0.225<e_T<2.0$ GeV. An event is excluded from the analysis if N_{tracks} or N_{clus} is below a minimum value to ensure that there are a sufficient number of tracks or clusters to determine a mean and to exclude background events. This minimum value for the 0–5 %, 0–10 %, 10–20 %, and 20–30 % centrality classes, respectively, is 40, 30, 20, and 10 for the M_{p_T} analysis and 30, 20, 10, and 10 for the M_{e_T} analysis. Table I lists statistics pertaining to the data samples used to determine M_{p_T} and Table II lists the statistics pertaining to the data samples used to determine M_{e_T}. The events used for the M_{p_T} and M_{e_T} analyses are considered independently of each other.

In order to compare the M_{p_T} and M_{e_T} distributions to what is expected for statistically independent particle emission, the baseline for the random distribution is defined by mixed events, which are events of multiplicity m assembled using individual tracks or clusters taken from a collection of m data events with one track or cluster taken from each data event. To obtain a precision comparison, it is important to match the number of tracks or clusters along with the mean of the semi-inclusive distribution of the mixed events to those of the data. Therefore, in both analyses, mixed events are constructed by predetermining the number of charged particle tracks or calorimeter clusters in the mixed event N_{mix} by directly sampling the corresponding data N_{tracks} or N_{clus} distributions. Figure 1 shows a comparison of the N_{tracks} distributions from the data and the normalized mixed event N_{mix} distribution for the 0–10 % centrality class. Once N_{mix} is determined, a mixed event is filled with p_T or e_T values from the data with the following criteria: (a) no two p_T or e_T values from the same data event are allowed to reside in the same mixed event, (b) only p_T or e_T values passing all cuts in the determination of M_{p_T} or M_{e_T} from the data events are placed in a mixed event, and (c) only data events from the same centrality class are used to construct a mixed event corresponding to that class. Once a mixed event is filled with N_{mix} tracks or clusters, its M_{p_T} or M_{e_T} is calculated in the same manner as for the data events.

For both analyses, the data contain a fraction of tracks or clusters within close physical proximity that have merged into a single track or cluster. This fraction is estimated by embedding simulated single-particle events that are processed through a detailed simulation of the detector response into real data events, which are then reconstructed in the same manner as the data. For the 0–5 % centrality class, we estimate that 6% of the tracks and 5% of the clusters are affected.

For the M_{p_T} analysis, tracks that are merged into a single reconstructed track typically have similar values of p_T. The result is a slightly lower value of N_{tracks} which causes a slight broadening in the width of the M_{p_T} distribution due to the reduced statistics per event. However, since the N_{tracks}

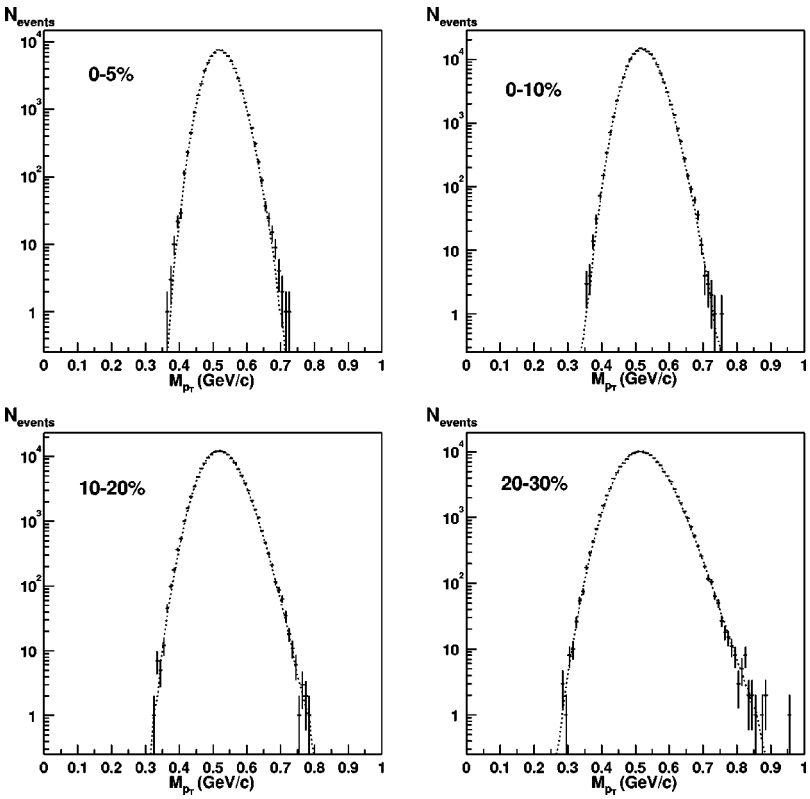

FIG. 3. The M_{p_T} distributions for all centrality classes. The curves are the random baseline mixed event distributions.

data distribution is directly sampled during the construction of mixed events, the effect of merged tracks cancels for comparisons between the data and mixed events.

For the M_{e_T} analysis, the effect of merged clusters is complicated by the fact that a single cluster is reconstructed with an e_T corresponding to the sum of the two (or more) particles contributing to the cluster. To understand this effect on the mixed events, we note that the fraction of merged clusters within a data event increases with event multiplicity. Also, many of the data events with the lowest M_{e_T} coincide with the lowest multiplicity events since they contain few, if any, merged clusters that would yield a higher M_{e_T}. When the merged clusters in the data events are randomly redistributed among the mixed events, low multiplicity mixed events can contain more merged clusters than the data events with the same multiplicity, resulting in a gross upward shift in M_{e_T} for those mixed events. This results in apparent excess nonrandom fluctuations at low M_{e_T}. Conversely, high multiplicity mixed events can contain fewer merged clusters than the data events with the same multiplicity, resulting in a gross downward shift in M_{e_T} for those mixed events. However, since the mean is taken over more clusters in this case, the effective shift in M_{e_T} is reduced at high M_{e_T}, and the apparent nonrandom fluctuations are much less pronounced. An estimate of the magnitude of this effect is presented later.

III. RESULTS

To compare directly the semi-inclusive p_T distribution to the M_{p_T} distribution assuming a statistically independent particle emission, the closed form prescription outlined in [15] is used. This prescription describes the semi-inclusive p_T distribution using a Gamma distribution,

$$f(p_T)=f_\Gamma(p_T,p,b)=\frac{b}{\Gamma(p)}(bp_T)^{p-1}e^{-bp_T}, \quad (3.1)$$

where p and b are free parameters that are related to the mean and standard deviation of the semi-inclusive distribution as

$$p=\frac{\langle p_T\rangle^2}{\sigma^2_{p_T}}, \quad b=\frac{\langle p_T\rangle}{\sigma^2_{p_T}}, \quad (3.2)$$

where

$$\sigma_{p_T}=(\langle p_T^2\rangle-\langle p_T\rangle^2)^{1/2}. \quad (3.3)$$

The reciprocal of b is the inverse slope parameter of the p_T distribution. With the track multiplicity distribution assumed to be a negative binomial distribution, $f_{NBD}(N_{tracks},1/k,\langle N_{tracks}\rangle)$, the M_{p_T} distribution can be calculated using

$$g(p_T)=\sum_{N=N_{min}}^{N_{max}} f_{NBD}(N,1/k,\langle N\rangle)f_\Gamma(p_T,Np,Nb), \quad (3.4)$$

where the sum is over N_{tracks} from N_{min} to N_{max}, which are the limits of the multiplicity. The value of the negative binomial distribution parameter k is given by

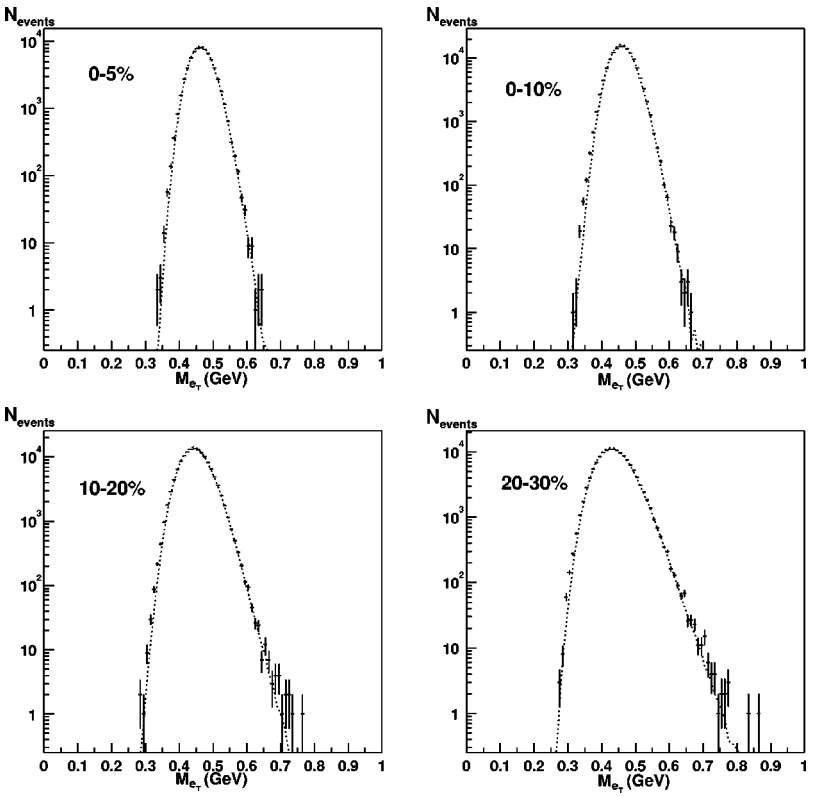

FIG. 4. The M_{e_T} distributions for all centrality classes. The curves are the random baseline mixed event distributions. The source of differences in the data and mixed event distributions are addressed in the text.

$$\frac{1}{k} = \frac{\sigma_{p_T}^2}{\langle N_{tracks} \rangle^2} - \frac{1}{\langle N_{tracks} \rangle}. \tag{3.5}$$

Therefore, given $\langle p_T \rangle$, σ_{p_T}, and $\langle N_{tracks} \rangle$ extracted from the semi-inclusive p_T distribution, the expected random M_{p_T} distribution can be calculated. Figure 2 shows the M_{p_T} distribution for the 0–5 % centrality class. Overlaid on the data as a dotted curve is the result of the calculation. The agreement between the data distribution and the calculation illustrates the absence of large nonstatistical fluctuations in the data. The remainder of this paper will quantify the amount of non-

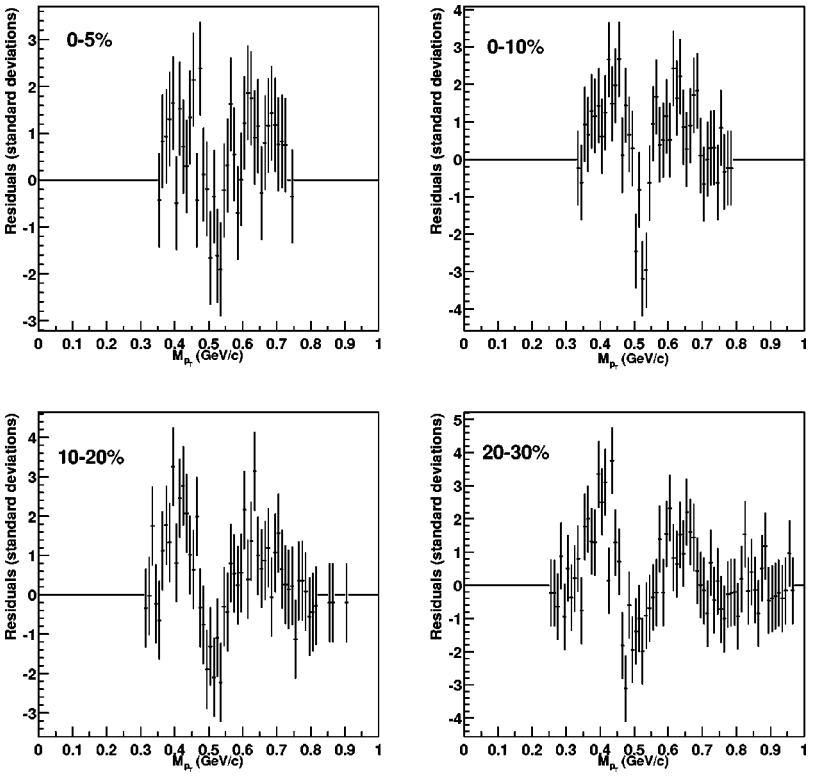

FIG. 5. The residual distribution between the data and mixed event M_{p_T} spectra as a function of M_{p_T} in units of standard deviations for all centrality classes. The total χ^2 and the number of degrees of freedom for the 0–5 %, 0–10 %, 10–20 %, and 20–30 % centrality classes are 89.0/37, 155.7/40, 163.3/47, and 218.4/61, respectively.

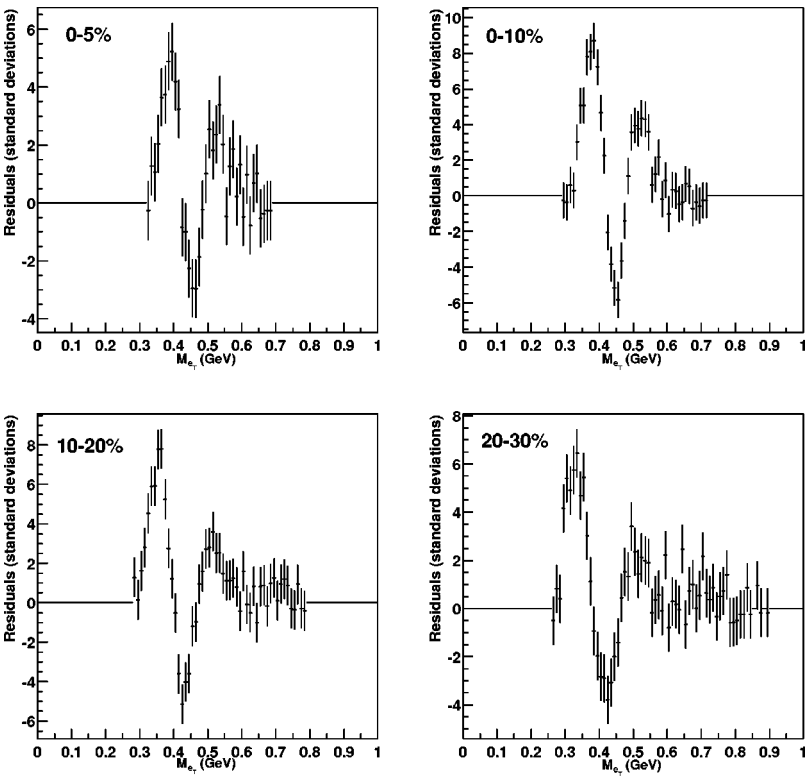

FIG. 6. The residual distribution between the data and mixed event M_{e_T} spectra as a function of M_{e_T} in units of standard deviations for all centrality classes. The total χ^2 and the number of degrees of freedom for the 0–5 %, 0–10 %, 10–20 %, and 20–30 % centrality classes are 310.0/32, 896.4/36, 678.7/47, and 553.9/53, respectively. A large fraction of the residual contributions are due to the effects of cluster merging.

statistical fluctuations observed and place limits on the level of fluctuations that can be present in central Au+Au collisions at $\sqrt{s_{NN}}=130$ GeV.

To quantify the magnitude of the deviation of fluctuations from the expectation of statistically independent particle emission, the magnitude of the fluctuation ω_T in the transverse quantity M_T, representing M_{p_T} or M_{e_T}, is defined as

$$\omega_T=\frac{(\langle M_T^2\rangle-\langle M_T\rangle^2)^{1/2}}{\langle M_T\rangle}=\frac{\sigma_{M_T}}{\langle M_T\rangle}. \tag{3.6}$$

The value of ω_T is calculated independently for the data distribution and for the baseline, or mixed event, distribution. The difference in the fluctuation from a random baseline distribution is defined as

$$d=\omega_{(T,data)}-\omega_{(T,baseline)}. \tag{3.7}$$

The sign of d is positive if the data distribution contains a correlation, such as Bose-Einstein correlations [16], when compared to the baseline distribution. The fraction of fluctuations that deviate from the expectation of statistically independent particle emission is given by

$$F_T=\frac{(\omega_{(T,data)}-\omega_{(T,baseline)})}{\omega_{(T,baseline)}}=\frac{(\sigma_{(T,data)}-\sigma_{(T,baseline)})}{\sigma_{(T,baseline)}}, \tag{3.8}$$

where $\sigma_{(T,\ data)}$ refers to the standard deviation of the event-by-event M_T data distribution and $\sigma_{(T,\ baseline)}$ is the corresponding quantity for the baseline, or mixed event, distribution. In the absence of a common language for the analysis of M_{p_T} and M_{e_T} fluctuations, the commonly used fluctuation quantity ϕ_T [17] is also presented in order to compare this measurement to previous results [5]. The quantity d is related directly to ϕ_T via

$$\phi_T=(\sigma_{(T,data)}-\sigma_{(T,baseline)})\sqrt{\langle N_T\rangle}=d\langle M_T\rangle\sqrt{\langle N_T\rangle}, \tag{3.9}$$

where N_T represents N_{tracks} or N_{clus}. The quantity ϕ_T is related to F_T by

$$\phi_T=F_T\sigma_{(T,baseline)}\sqrt{\langle N_T\rangle}. \tag{3.10}$$

TABLE III. Fluctuation quantities for the M_{p_T} analysis.

Centrality	0–5 %	0–10 %	10–20 %	20–30 %
$\omega_{(T,data)}$(%)	7.37±0.10	7.85±0.13	9.52±0.14	11.7±0.21
d(%)	0.14±0.15	0.16±0.19	0.19±0.21	0.21±0.35
F_T(%)	1.9±2.1	2.0±2.5	2.1±2.2	1.8±3.0
ϕ_{p_T} (MeV/c)	5.65±6.02	6.03±7.28	6.11±6.63	5.47±9.16

TABLE IV. Fluctuation quantities for the M_{e_T} analysis.

Centrality	0–5 %	0–10 %	10–20 %	20–30 %
$\omega_{(T,data)}$(%)	7.32±0.07	7.84±0.08	9.58±0.17	11.8±0.26
d(%)	0.30±0.09	0.37±0.12	0.38±0.20	0.40±0.32
F_T(%)	4.3±1.3	5.0±1.6	4.2±2.2	3.5±2.8
ϕ_{e_T} (MeV)	11.5±3.59	13.6±4.23	11.1±5.75	9.28±7.34

The standard deviation of the semi-inclusive spectra can be approximated by $\sigma_{(T,incl.)} \approx \sigma_{(T,baseline)} \sqrt{\langle N_T \rangle}$ [15], where $\sigma_{(T,incl.)}$ is the standard deviation of the semi-inclusive distribution as defined in Eq. (3.3). Therefore, ϕ_T is simply the fraction of nonrandom fluctuations in the event-by-event mean p_T or e_T, F_T, scaled by $\sigma_{(T,incl.)}$. An advantage of F_T over ϕ_T is that measurements expressed in F_T can be directly compared without further scaling.

The magnitudes of any nonrandom fluctuations are established by comparing the data distributions to the mixed event distributions, which serve as the random baseline distributions. For this purpose, the mixed event distributions are normalized to minimize the χ^2 value with respect to the data distributions. Figures 3 and 4 show the M_{p_T} and M_{e_T} distributions for all four centrality classes (data points) with the corresponding mixed event M_{p_T} and M_{e_T} distributions overlayed on the data as dotted curves. The broadening of the distributions for less central collisions are due to the reduction in $\langle N_{tracks} \rangle$ or $\langle N_{clus} \rangle$. Shown in Fig. 5 and Fig. 6 are the residuals between the data and mixed events, defined for each bin i as residual$_i = (M_{(T,data)_i} - M_{(T,mixed)_i})/\sigma_i$, in units of standard deviations, for each centrality class. The shapes of the residual distributions are primarily driven by the normalization procedure applied to the mixed events.

For the M_{p_T} distributions, the data and mixed event distributions are indistinguishable. However, the upper M_{e_T} edges of the data and mixed event M_{e_T} distributions show good agreement while the lower M_{e_T} edge of the data distributions are slightly wider than the mixed event distribution. If this low e_T effect were physical, it would imply fluctuations with slightly more low e_T photons since the effect is not seen in the M_{p_T} distribution for charged particle tracks. However, some of the excess fluctuations at low e_T can be attributed to the effects of cluster merging previously discussed. The magnitude of this effect has been investigated using a Monte Carlo simulation which calculates M_{e_T} after reproducing the calorimeter cluster separation distribution, the N_{clus} distribution, and the semi-inclusive e_T distributions from the data. The fluctuations in the M_{e_T} distribution with this effect included in each event are compared to a simulated mixed event M_{e_T} distribution constructed from the same generated data set using the same procedure that is applied to the data. In this manner, it is estimated that the cluster merging effect contributes an additional $F_T = 1.5\%$, 2.1%, 0.9%, and less than 0.01% to the nonrandom fluctuations for the 0–5 %, 0–10 %, 10–20 %, and 20–30 % centrality classes, respectively. The simulation confirms that the cluster merging effect significantly contributes only to the lower M_{e_T} edge of the distribution. The remainder of the excess low e_T fluctuations is likely due to correlated low energy background. GEANT [19] simulations indicate that the primary background contribution is produced by low energy electrons and muons that scatter off the pole tips of the central arm spectrometer magnet but still pass the cluster selection cuts. Because of the difficulty in quantifying the contribution of background to the excess fluctuations, the present M_{e_T} data are taken to indicate an upper limit on nonstatistical fluctuations rather than an indication of true nonstatistical fluctuations.

The values of ω_T, d, F_T, and ϕ_T for each centrality class using the mixed events as the random baseline distribution are tabulated in Table III for M_{p_T} and Table IV for M_{e_T}. The errors quoted for these quantities include statistical errors and systematic errors due to time-dependent variations over the data-taking period. The systematic errors are estimated by dividing each data set into nine subsets with each subset containing roughly equal numbers of events. For the M_{p_T} analysis, the systematic errors contribute to 81%, 88%, 76%, and 75% of the total error in ω_T and 85%, 88%, 80%, and 85% of the total error in the variables d, F_T, and ϕ_t for the 0–5 %, 0–10 %, 10–20 %, and 20–30 % centrality classes, respectively. The corresponding values for the M_{e_T} analysis are a 67%, 63%, 81%, and 82% contribution to the total errors in ω_T, and a 64%, 63%, 81%, and 82% contribution to the total errors in d, F_T, and ϕ_t for each centrality class. The cluster merging contribution estimates noted above are not applied to the values quoted in Table IV.

IV. DISCUSSION

Based upon the fluctuation measurements presented here, certain fluctuation scenarios in RHIC Au+Au collisions at $\sqrt{s_{NN}} = 130$ GeV are excluded. For this purpose, we consider two variations of a model that contains two classes of events with a difference of effective temperature, defined as $\Delta T = T_2 - T_1$, where T_2 is the inverse slope parameter of the event class with the higher effective temperature, and T_1 is the inverse slope parameter of the event class with the lower effective temperature. The first variation, model A, will consider a case where the means of the semi-inclusive p_T spectra for the two event classes are identical, but the standard deviations are different. The second variation, model B, will consider a case where the means of the semi-inclusive p_T spectra are different, but the standard deviations are identical. Since the semi-inclusive p_T distribution is an observed

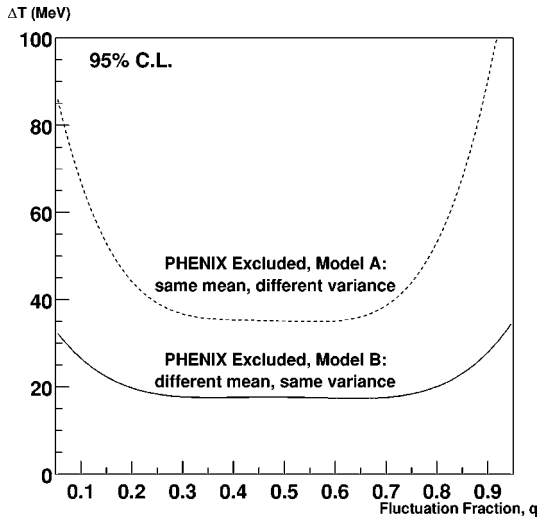

FIG. 7. The PHENIX sensitivity to nonrandom fluctuations in the two variations of the dual event class model that are excluded at the 95% confidence level by the M_{p_T} analysis in the 0–5 % centrality class. The fraction of events q in the class of events with the lower inverse slope parameter (event class 1) is plotted on the horizontal axis while the difference in inverse slope parameter between event class 1 and event class 2, ΔT, is plotted on the vertical axis. The curves represent the lower boundaries of the excluded regions.

quantity, the two event classes must be constrained in such a way that the mean and standard deviation of the final semi-inclusive p_T distribution remain constant while the effect of the fluctuation manifests itself in the M_{p_T} distribution.

The dual event class model is applied to the determination of the sensitivity to fluctuations in M_{p_T} for the 0–5 % centrality class as follows. Returning to the prescription outlined in [15], the semi-inclusive transverse p_T spectrum can be parametrized by the $f_\Gamma(p_T,p,b)$ distribution defined in Eq. (3.1). For both model variations, the fraction of events in the event class with the higher effective temperature is defined as

$$q=\frac{(N_{events})_{class\ 1}}{(N_{events})_{class\ 1}+(N_{events})_{class\ 2}}. \tag{4.1}$$

The p_T distribution of the combined sample can then be expressed as

$$f(p_T)=q\Gamma(p_T,p_1,b_1)+(1-q)\Gamma(p_T,p_2,b_2), \tag{4.2}$$

where $T_1=1/b_1$ and $T_2=1/b_2$.

For model A, the semi-inclusive p_T distributions of each event class are constrained to have the same mean, so we require

$$\mu=p/b=p_1/b_1=p_2/b_2. \tag{4.3}$$

The variance of the final semi-inclusive p_T distribution for model A is constrained by

$$\frac{\sigma^2}{\mu^2}=\frac{1}{p}=\frac{q}{p_1}+\frac{(1-q)}{p_2}. \tag{4.4}$$

With these constraints, the choice of a value for q and the effective temperature of one event class is sufficient to extract the remaining parameters from which sensitivity estimates for fluctuations in M_{p_T} are obtained.

For model B, the semi-inclusive p_T distributions of each event class are allowed to have different means, μ_1 and μ_2, so the mean of the total semi-inclusive distribution can be expressed as $\mu=q\mu_1+(1-q)\mu_2$. Defining a mean shift $\Delta\mu$ as $\Delta\mu=\mu_2-\mu_1$, we obtain

$$\mu_2=\mu+q\Delta\mu. \tag{4.5}$$

Allowing $p_1=p_2$ and applying the constraint that the variances of the two event classes are identical, yields

$$\frac{1}{p_1}=\frac{1/p-q(1-q)(\Delta\mu/\mu)^2}{1+q(1-q)(\Delta\mu/\mu)^2}. \tag{4.6}$$

With a choice of values for q and $\Delta\mu$, the remaining parameters can be calculated, including ΔT.

Both variations of the dual event class model are implemented in a Monte Carlo simulation in the following manner. The number of particles in an event is determined by sampling the N_{tracks} data distribution, approximated by a Gaussian distribution fit to the data. The p_T of each particle in an event is determined individually by sampling the appropriate $\Gamma(p_T,p,b)$ distribution fit to the semi-inclusive p_T data distribution, which yields $p=0.8$ and $b=2.46$ for 0–5 % centrality. The p_T of each particle is restricted to the p_T range of the measurement. With N_{tracks} and the p_T distribution determined, the M_{p_T} for a given number of events is calculated. The generated M_{p_T} distribution with $q=0$ for either model variation is found to be statistically consistent with the mixed event M_{p_T} distribution.

The data contain a fraction of background particles that did not originate from the collision vertex that effectively dilute the sensitivity to nonrandom fluctuations. To address this, a fraction of the particles in an event are randomly tagged as background particles, whose p_T distribution is then generated with a separate parametrization prior to calculating M_{p_T} for an event. The level of background contamination is estimated by processing HIJING [18] Au+Au events through a software chain that includes a detailed GEANT simulation [19] with the complete PHENIX detector geometry included, followed by a detailed simulation of the detector electronics response [12], whose output is then processed by track, cluster, and momentum reconstruction using the identical software and input parameters as is used for the data analysis. It is estimated that 11% of the tracks and 26% of the clusters are due to background particles, independent of centrality class over the centrality range of these measurements. The estimated p_T and e_T distributions for the background particles are well parametrized by exponential distributions. Again, the majority of the e_T background occurs at low e_T, so any correlated background would most likely contribute to the lower side of the M_{e_T} distribution.

To determine the sensitivity to fluctuations within the dual event class model, the fluctuation fraction q and the value of p_1 for model A and $\Delta\mu$ for model B are varied and the M_{p_T} distribution is generated at each step. A χ^2 test is then performed on the generated M_{p_T} distribution with respect to the mixed event data M_{p_T} distribution. For a given value of q, the χ^2 result increases as ΔT increases, which allows a fluctuation exclusion region to be defined for the single degree of freedom. The curves in Fig. 7 show the lower exclusion boundaries for the 0–5 % centrality M_{p_T} measurement at the 95% confidence level as a function of q and ΔT for both variations of the model. If the sensitivity is determined based upon the nonmixed data distribution, the lower exclusion boundary increases by less than 2 MeV for all values of q for either model. Also, for all values of q in either model, the estimated background contribution degrades the sensitivity estimates by $\Delta T = 3$ MeV for both models.

A recent model of event-by-event fluctuations where the temperature parameter $T = 1/b$ fluctuates with a standard deviation σ_T on an event-by-event basis [20] can be simply related to F_T:

$$\frac{\sigma_T^2}{\langle T\rangle^2} = \frac{2F_T}{p(\langle n\rangle - 1)}, \tag{4.7}$$

where $p = 0.8$ is the semi-inclusive parameter extracted from the present data. For the 0–5 % centrality class, the present measurement establishes a 95% confidence limit of 2.6×10^{-3} for $\sigma_T^2/\langle T\rangle^2$, or 5% for $\sigma_T/\langle T\rangle$.

V. CONCLUSIONS

The fluctuations in the M_{p_T} distributions for all centrality classes are consistent with the presence of no fluctuations in excess of the random expectation. The magnitude of F_T in all cases is positive, which may be due to the presence of Hanbury-Brown-Twiss correlations. The fluctuations in the M_{e_T} distributions do have a small nonstatistical component, much of which is attributable to the effects of merged clusters, the remainder of which are taken to indicate an upper limit on nonstatistical fluctuations in transverse energy. By defining a dual event class model, limits are set on the amount of M_{p_T} fluctuations that can be present in the angular aperture $|\eta| < 0.35$ and $\Delta\phi = 58.5°$ in $\sqrt{s_{NN}} = 130$ GeV Au+Au collisions. During the RHIC run of 2001, PHENIX has taken data for $\sqrt{s_{NN}} = 200$ GeV Au+Au collisions with about a factor of 4 increase in azimuthal angular acceptance for both the M_{p_T} and M_{e_T} analyses, which will allow the measurements to be extended toward more peripheral collisions.

ACKNOWLEDGMENTS

We thank the staff of the RHIC project, Collider-Accelerator, and Physics Departments at BNL and the staff of PHENIX participating institutions for their vital contributions. We acknowledge support from the Department of Energy and NSF (USA), Monbu-sho and STA (Japan), RAS, RMAE, and RMS (Russia), BMBF, DAAD, and AvH (Germany), FRN, NFR, and the Wallenberg Foundation (Sweden), MIST and NSERC (Canada), CNPq and FAPESP (Brazil), IN2P3/CNRS (France), DAE (India), KRF and KOSEF (Korea), and the U.S.-Israel Binational Science Foundation.

[1] H. Heiselberg, Phys. Rep. **351**, 161 (2001).
[2] S. Mrowczynski, Phys. Lett. B **314**, 118 (1993).
[3] M. Stephanov, K. Rajagopal, and E. Shuryak, Phys. Rev. Lett. **81**, 4816 (1998).
[4] A. Dumitru and R. Pisarski, Phys. Lett. B **504**, 282 (2001).
[5] H. Appelshauser *et al.*, Phys. Lett. B **459**, 679 (1999).
[6] S. V. Afanasiev *et al.*, Phys. Rev. Lett. **86**, 1965 (2001).
[7] D. P. Morrison *et al.*, PHENIX Collaboration, Nucl. Phys. **A638**, 565c (1998).
[8] K. Ikematsu *et al.*, Nucl. Instrum. Methods Phys. Res. A **411**, 238 (1998).
[9] C. Adler, A. Denisov, E. Garcia, M. Murray, H. Strobele, and S. White, Nucl. Instrum. Methods Phys. Res. A **461**, 337 (2001).
[10] K. Adcox *et al.*, PHENIX Collaboration, Phys. Rev. Lett. **86**, 3500 (2001).
[11] V. Riabov *et al.*, Nucl. Instrum. Methods Phys. Res. A **419**, 363 (1998).
[12] J. T. Mitchell *et al.*, Nucl. Instrum. Methods Phys. Res. A **482**, 491 (2002).
[13] G. David *et al.*, IEEE Trans. Nucl. Sci. **45**, 692, 705 (1998).
[14] K. Adcox *et al.*, PHENIX Collaboration, Phys. Rev. Lett. **87**, 052301 (2001).
[15] M. J. Tannenbaum, Phys. Lett. B **498**, 29 (2001).
[16] U. Wiedemann and U. Heinz, Phys. Rep. **319**, 145 (1999).
[17] M. Gazdzicki and S. Mrowczynski, Z. Phys. C **54**, 127 (1992).
[18] X-N. Wang and M. Gyulassy, Phys. Rev. D **44**, 3501 (1991).
[19] R. Brun and F. Carminati, CERN Program Library, Long Writeup W5013, 1994.
[20] R. Korus and S. Mrowczynski, Phys. Rev. C **64**, 054908 (2001).